SMAR 2017 – Fourth Conference on Smart Monitoring,
Assessment and Rehabilitation of Civil Structures

Assessment of axial behavior of HPFRCC members externally confined with FRP sheets

Ugur Demir[1], Medine Ispir[1], Yusuf Sahinkaya[1] and Alper Ilki[1]

[1] Istanbul Technical University, Istanbul, Turkey

ABSTRACT: The aim of this paper is to identify the axial behavior characteristics of FRP (fiber reinforced polymer) confined HPFRCC (high performance fiber reinforced cementitious composite) members under compression. Early results of a more comprehensive project obtained for 12 HPFRCC specimens with circular, square or rectangular cross-sections are outlined in this paper. The average compressive strength of the specimens was 102.4 MPa, 106.6 MPa and 94.2 MPa for circular, square and rectangular specimens, respectively. The test program comprised of 2 FRP confined and 2 unconfined specimens for each cross-section type (circular, square and rectangular) where carbon FRP sheets were used for external confinement. Transverse confinement generated by external FRP sheets resulted with a remarkable enhancement in axial strength and deformability, which is extremely important to compensate seismic actions. While contribution of external FRP confinement was remarkable for all types of sections, particularly in terms of deformability, FRP confined circular HPFRCC specimens demonstrated relatively better performance in terms of strength in accordance with the uniform stress distribution arising from their shapes. Test results of specimens with square and rectangular cross-section also shed some light on the effects of section geometry on the axial behavior of FRP confined HPFRCC members. After presenting experimental work, several available models proposed for predicting the axial behavior of FRP jacketed conventional concrete were examined by comparing their estimations with the test data. This comparison showed that the predictions of some investigated models are in good agreement with the test results.

1 INTRODUCTION

Decreasing the dimensions of structural members and their self-weights, may result in feasible architectural solutions. In such cases, use of high strength concrete (HSC) in the construction industry has been a promising approach. However, decreasing the dimensions and increasing the strength of concrete generally cause brittleness which should be avoided in design of concrete structures. In order to eliminate this drawback in higher strength concretes, one solution is adding steel fibers for achieving a more ductile behavior.

The new kind of cementitious compounds containing fibers and small size aggregates such as silica fume, fly ash, slags, etc. are called as high performance fiber reinforced cementitious composites (HPFRCC). Nowadays, HPFRCCs are used in high-rise buildings, long-span bridges, highways, and airfield pavements (Brandt, 2008). When compared to conventional concrete, HPFRCCs are remarkably better in terms of strength, and durability characteristics obtained from low water/cement ratios and higher tensile strengths. Besides, HPFRCCs may demand additional ductility depending on the mix composition and this demand can be fulfilled by lateral confinement. This confinement can be provided by fiber reinforced polymers (FRP) with the aim of a more ductile behavior. Contribution of external FRP confinement in transverse direction to strength and deformation capacities of columns was verified by many researchers mainly focusing on normal strength concrete (NSC) (e.g. Teng et al. 2002; Bakis

et al. 2002; Ilki et al. 2002, 2004, 2008; Dai et al. 2011, Wang et al. 2016). A limited number of researchers investigated the contribution of FRP jacketing in case of HSC (Mandal et al. 2005; Almusallam et al. 2007; Wu et al. 2009; Ozbakkaloglu 2012; Ozbakkaloglu et al. 2016) while studies on FRP confined concrete with steel fiber content are extremely rare (Zohrevand and Mirmiran 2012; Xie and Ozbakkaloglu 2015). Zohrevand and Mirmiran (2012) demonstrated the benefits of using ultra-high performance concrete (UHPC) filled FRP tubes with circular cross-section. The unconfined compressive strength of the specimens was measured as 189 MPa. Specimens were confined by glass (GFRP) or carbon fiber reinforced polymer (CFRP) tubes. Xie and Ozbakkaloglu (2015) presented an experimental study on the axial compressive behavior of steel fiber reinforced high strength concrete (SFRHSC) filled FRP tubes and slurry infiltrated fiber concrete (SIFCON) filled FRP tubes with circular cross-sections. However, both studies investigated the axial behavior of the specimens with circular cross-section.

In the light of the literature review, the axial behavior of HPFRCC specimens with circular, square and rectangular cross sections externally confined by FRP jackets was investigated through testing. It should be should clarified that this research deals with confinement of a high performance cementitious composite and not a concrete, since there is no coarse aggregate in the mix. Available analytical models applicable to FRP confined conventional concrete are also assessed in terms of predicting the axial behavior of HPFRCC specimens jacketed with FRP.

2 EXPERIMENTAL WORK

Twelve HPFRCC specimens with 3 different cross-sections (circular, square and rectangular) were produced. Cross sectional dimensions were 150 mm of diameter for circular specimens, 150 mm x 150 mm for square specimens and 150 mm x 225 mm for rectangular ones. All specimens had the height of 300 mm. Corners were rounded to 25 mm radius for both square and rectangular specimens to reduce stress concentrations around the corners. The test program comprised of 2 confined with 2 plies of FRP and 2 unconfined specimens for each cross-section type (a total of 4 circular, 4 square and 4 rectangular) where carbon FRP sheets were used for external confinement. Compressive strength was obtained 102.4 MPa, 106.6 MPa and 94.2 MPa for circular, square and rectangular specimens, respectively. The average axial strains at peak stress were calculated as 0.0032, 0.0035 and 0.0030 for circular, square and rectangular specimens, respectively. Details of the test specimens are summarized in Table 1. In this table, "CC" is used for cementitious composite, "C", "S" and "R" are used for circular, square and rectangular cross sections, respectively. The volumetric ratio of FRP (ρ_f) values seen in Table 1 were calculated using Eq. (1) for circular specimens and Eq. (2) for square and rectangular ones as recommended by Ilki et al. (2004). In Eqs. 1 and 2, t_f is the total effective thickness of FRP, D is the diameter of the circular specimens, b and h are the width and the depth of the cross section in square and rectangular specimens.

$$\rho_f = \frac{4t_f}{D} \tag{1}$$

$$\rho_f = \frac{2t_f\,(\mathrm{b}+\mathrm{h})}{bh} \tag{2}$$

HPFRCC specimens were produced by a local concrete supplier (ISTON). Mix proportions of cementitious composite are given in Table 2. Nominal maximum size of sand was 0.5 mm and no coarse aggregate was used. Steel fibers were 0.9 mm in diameter and 60 mm in length, referring to an aspect ratio of 67 (length / diameter). The steel fiber volume fraction V_f (i.e. volume of fibers per unit volume of concrete) was 1%. The amount of silica fume was 25% of the binder (cement) by weight. Mechanical properties of unidirectional CFRP sheets provided by the manufacturer are given in Table 3. The epoxy

used for bonding CFRP sheets consisted of a resin binder and hardener, which are mixed, in a ratio of 2/1 by weight. Density and viscosity of the epoxy-binder mix given by manufacturer are 1.05 kg/lt and 500 cp, respectively.

Table 1. Details of test specimens

Designation	Number of specimens	Section geometry	Number of CFRP plies	FRP volumetric ratio (ρ_f)
CC-C–0	*2*	Circular	Unconfined	-
CC-C–2	*2*	Circular	2	0.009
CC-S–0	*2*	Square	Unconfined	-
CC-S–2	*2*	Square	2	0.009
CC-R–0	*2*	Rectangular	Unconfined	-
CC-R–2	*2*	Rectangular	2	0.007

Table 2. Mix proportions of cementitious composite (kg/m^3)

C	*SF*	*S*	*STF*	*W*	*SP*	*Total*
1000	250	815	78.5	124	125	2392.5

***C**: Cement (CEM I 42.5R) **SF**: Silica Fume (Norchem) **S**: Sand (0-0.5 mm) **STF**: Steel Fiber (Dramix, 60 mm, hooked-end) **W**: Water **SP**: Superplastisizer (Chryso Optima 208)*

Table 3. Mechanical properties of CFRP sheets given by manufacturer

Tensile Strength (MPa)	Tensile Elasticity Modulus (MPa)	Ultimate Tensile Deformation (%)	Effective Thickness (mm)
4200	240000	1.8	0.166

Jacketing of HPFRCC specimens was executed in five steps as 1) cleaning of surface of each specimen, 2) primer coating to specimen surface, 3) epoxy applying over primer, 4) CFRP sheet application over epoxy, and 5) forming an overlap of 150 mm at the end of FRP jacket. After jacketing process is completed, the specimens were left in laboratory for at least a week to ensure the proper curing of epoxy before testing. Compression tests were carried out under monotonic uniaxial compressive loading by using an Instron testing machine with a capacity of 5000 kN. The tests were displacement controlled with a loading rate of 0.5 mm per minute. For measuring the axial deformations, 2 linear variable differential transducers (LVDTs) for circular specimens and four LVDTs (one per each face of the specimen) for square and rectangular specimens were located at the mid height of the specimen with a gauge length of 150 mm (Fig. 1). Additionally, two LVDTs were placed between the loading and supporting steel plates along the height of the specimen (Fig. 1). To measure the lateral strains, for all specimens, strain gauges were placed along the transverse direction. The gage length of each strain gage was 60 mm and the strain gages were placed at the mid-height of the specimen. A TML-TDS-303 data logger was used for data acquisition. Axial loads applied were taken directly from the built-in load cell of the Instron testing machine. The axial behavior of unconfined and externally jacketed HPFRCC specimens can be presented with stress-strain relationships. These relationships are given in Fig. 2 and Table 4. In these plots, the negative parts of the horizontal axis are used to show lateral strains whereas positive parts are used for axial strains (ε_c). In Table 4, f'_{co} and f'_{cc} are the unconfined and confined axial strengths, while ε_{co} and ε_{cu} are the ultimate axial strains for the unconfined and confined specimens, respectively. $\varepsilon_{h,rup}$ is the hoop rupture strain. It should be noted that, in this paper, the ultimate axial strain is the strain at which sudden rupture of FRP occurs (Fig.2). Axial stresses were computed by dividing the recorded loads to the cross section area of the specimen tested. The axial strains were

calculated by dividing the average displacement readings of the LVDTs at mid-height to the gage length of 150 mm.

a) b) c)

Fig. 1. Test setup for a) circular b) square and c) rectangular specimens illustrating LVDT and strain gauge application

In Fig. 2, it can be clearly noticed that both the axial stress and strain at failure for the confined columns were higher than those for the unconfined ones and the highest values for strength enhancement were obtained for confined circular columns (Fig. 2b), whereas the CFRP confined rectangular specimens exhibited more remarkable strain enhancements (Fig. 2f). As seen in Fig. 2b, 2d and 2f, the stress-strain relationships of FRP confined HPFRCC specimens are different from those of FRP confined conventional concrete. As seen in Fig. 2, FRP confined HPFRCC stress-strain behavior can be represented by a first ascending branch followed by a descending branch and in most cases with a second ascending branch before failure. The reference specimens exhibited a significantly brittle behavior after reaching peak stress (Fig 2a, 2c, 2e). On the other hand, when properly confined with external FRP jackets, the deformation capacity of the specimens improves significantly (Figs. 2b-d and 3b-f). As seen in figures, the specimens exhibited a softening behavior after the first peak, which is followed by an increase on resisted axial force until failure. The authors think that the reduction in axial load bearing capacity after the first peak would be less, when volumetric ratio of FRP is stronger corresponding to a higher confinement ratio which is discussed at following section. The slopes of the first ascending branches are similar for all unconfined and FRP jacketed specimens. This shows that the unconfined cementitious composite material properties govern the behavior in this range. However, the descending and the second ascending branches are affected by the axial stiffness of CFRP jacket. As seen in Fig. 2 and Table 4, the effect of FRP confinement on deformability is much more pronounced than that on strength. Test results indicated that circular specimens exhibited more remarkable strength enhancement with respect to square and rectangular ones. On the other hand, particularly for rectangular specimens, remarkable enhancement in ultimate strain is obtained with respect to circular and square ones. This behavior was also reported by Ilki et al. (2008) for CFRP confined low and medium strength concrete. Ilki et al. (2008) reported more remarkable strength enhancements for circular specimens and higher deformability for square and rectangular specimens. As seen in Table 4, strength enhancements in rectangular specimens are observed to be higher than that of square ones. The main reason of this behavior is attributed to the relatively lower unconfined strengths of rectangular specimens compared to square ones.

In HPFRCC specimens, due to the decrease in dilation capacity caused by the increase in compressive strength, lower transverse FRP strains were obtained resulting in smaller dilation capacities with respect to NSC. As seen in Table 4, for circular, square and rectangular specimens, confined with two layers of CFRP, axial strengths were enhanced by an average value of 45%, 15% and 13%, respectively, while ultimate axial strains were improved by 164%, 164% and 317% for circular, square and rectangular specimens, respectively. Consequently, it is apparent that external FRP jacketing significantly improves the deformation capacity of the HPFRCC specimens. This is particularly important for members to be subjected to seismic actions.

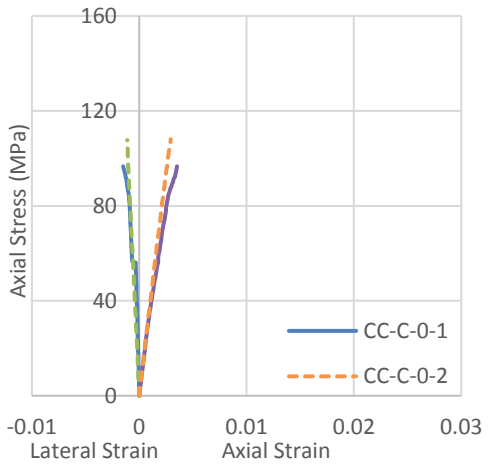

a)

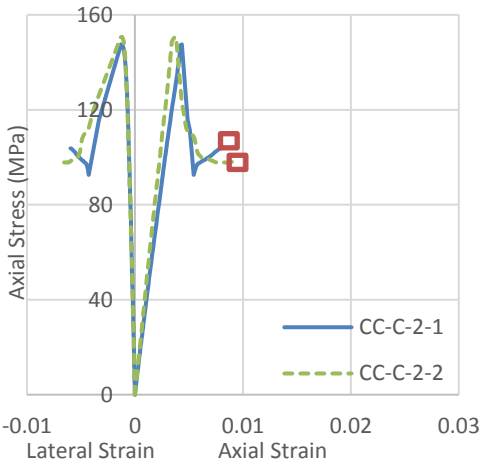

b)

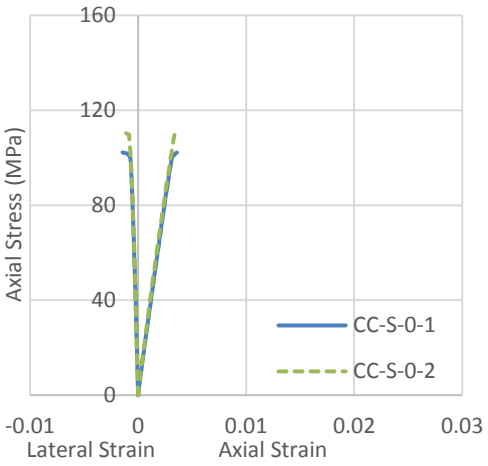

c)

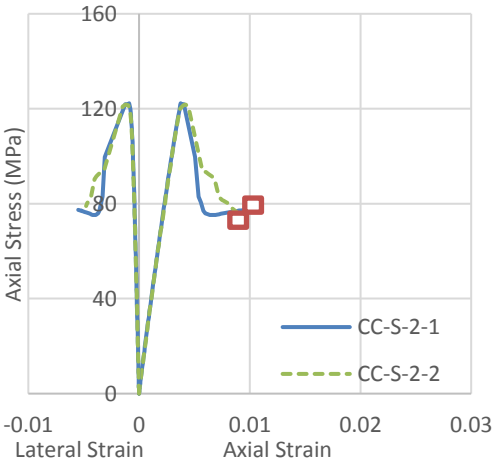

d)

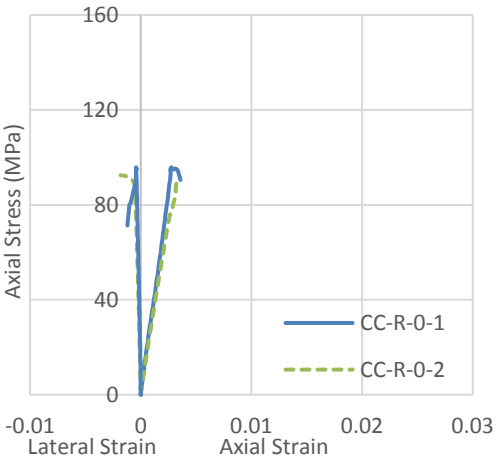

e)

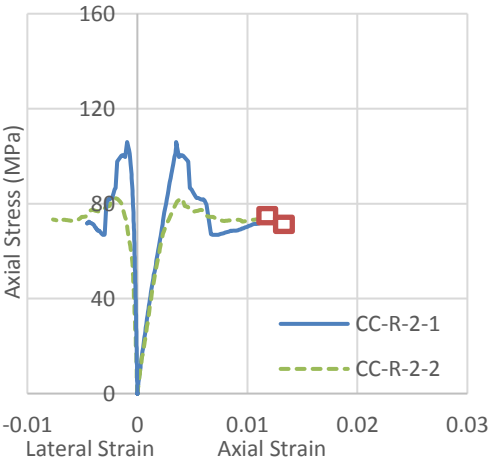

f)

Fig.2. Axial stress-axial strain and axial stress- lateral strain curves for a) unconfined circular, b) confined circular, c) unconfined square, d) confined square, e) unconfined rectangular, e) confined rectangular HPFRCC specimens
: Ultimate axial strain definition

Table 4. Experimental Test Results

Specimen	f'_{co} (MPa)	f'_{cc} (MPa)	ε_{co}	ε_{cu}	$\varepsilon_{h,rup}$	f'_{cc}/f'_{co}	$\varepsilon_{cu}/\varepsilon_{co}$	Average f'_{cc}/f'_{co}	Average $\varepsilon_{cu}/\varepsilon_{co}$
CC-C-0-1	96.7	x	0.0035	x	x	x	x	x	x
CC-C-0-2	108.1	x	0.0029	x	x	x	x		
CC-C-2-1	x	147.6	x	0.0079	0.006	1.44	2.47	1.45	2.64
CC-C-2-2	x	150.8	x	0.0090	0.007	1.47	2.81		
CC-S-0-1	102.2	x	0.0035	x	x	x	x	x	x
CC-S-0-2	110.6	x	0.0036	x	x	x	x		
CC-S-2-1	x	122.0	x	0.0096	0.005	1.15	2.74	1.15	2.64
CC-S-2-2	x	121.8	x	0.0089	0.005	1.14	2.54		
CC-R-0-1	95.8	x	0.0027	x	x	x	x	x	x
CC-R-0-2	92.5	x	0.0033	x	x	x	x		
CC-R-2-1	x	106.0	x	0.0125	0.005	1.13	4.17	1.13	4.17
*CC-R-2-2**	x	82.3	x	0.0117	0.007	0.87	3.90		

* Premature failure due to eccentric during loading. Excluded in calculation of the average values.

While the unconfined HPFRCC specimens fail in an extremely brittle manner, the FRP jacketed HPFRCC specimens display a limited and sudden post-peak strength loss and then an ascending second branch occurs. This strength loss is due to the lack of confinement effectiveness that could be eliminated using more amount of FRP volumetric ratio. The other reason is the use of low volume fraction of steel fibers (1%) for the production of the HPFRCC specimens in this study. Xie and Ozbakkaloglu (2015) stated that higher volume fraction of steel fibers (not less than 1.5%) can reduce the level of the strength loss right after the first peak for HSC. On the other hand, damage localization in HPFRCC which can be more severe with respect to NSC may have caused decreasing of hoop rupture strain of FRP jacket. The average value of the hoop rupture strain is obtained as 0.006 for all specimens independent from cross-sectional shape (Table 4). Using this average value, strain efficiency factor (k_ε), which is the ratio of the hoop rupture strain to the ultimate uniaxial tensile strain of FRP, is calculated as 0.30 for HPFRCC specimens. This value is less with respect to FRP confined NSC. The inverse relationship between unconfined concrete compressive strength and hoop rupture strain of FRP was also reported by Xiao et al. (2010), Ozbakkaloglu and Akin (2011), Zohrevand and Mirmiran (2011) and Lim and Ozbakkaloglu (2015).

Typical failure modes of specimens are shown in Fig. 3. All specimens failed with an explosive rupture of the jackets resulting in one vertical cut with a height of 150 to 200 mm. As seen in Fig. 3, this failure mode was characterized with a major crack at or near one of the corners of the specimens. The specimens, which displayed almost identical failure modes, reached similar FRP hoop rupture strains independent of FRP thickness, aspect ratio and shape.

(a) (b) (c)

Fig. 3. Typical failure modes of (a) circular, (b) square and (c) rectangular specimens

3 ANALYTICAL WORK

There is no model in the published literature, which has been proposed specifically to predict the axial behavior of FRP confined HPFRCC. Therefore, 5 existing models, which have been proposed for FRP confined normal or high strength concrete, are used to predict the confined strength and ultimate strain of FRP confined HPFRCC specimens. The formulations proposed by these models for prediction of FRP confined strength and ultimate axial strain are given in Table 5. Some of the investigated models are not directly applicable to noncircular sections. In order to use these models for noncircular sections, the equivalent sectional diameter definition given by Lam and Teng (2003) is taken into account, Eq. (3), where *D*, *b* and *h* are equivalent diameter, width and depth of the specimen, respectively.

$$D = \sqrt{b^2 + h^2} \tag{3}$$

The predictions of the models are plotted in Figs. 4 and 5 for axial strength and ultimate axial strain, respectively. It should be noted that in Figs. 4 and 5, the horizontal and vertical axes refer to analytically predicted and experimentally obtained enhancement ratios, respectively. In order to evaluate the confined strength and ultimate strain predictions of the models statistically, the average absolute error (*AAE*) and standard deviation (*SD*) are calculated using Eqs. (4 and 5). In these equations, mod_i and exp_i indicate the predicted value by the model and the corresponding value determined by the test, respectively; mod_{avg} and exp_{avg} are the average values predicted by the model and determined by the test, respectively; and *n* is the number of test. Table 6 presents the *AAE* and *SD* values calculated for each model. Wu and Zhou (2010) have defined the accuracy of a model based on *AAE* value; Category I ($AAE \leq 0.15$), Category II ($0.15 < AAE \leq 0.30$) and Category III ($AAE > 0.30$). The strength and ultimate strain predictions of the investigated models are categorized using this approach (Table 7).

$$AAE = \frac{\sum_{i=1}^{n} \left| \frac{\text{mod}_i - \text{exp}_i}{\text{exp}_i} \right|}{n} \tag{4}$$

$$SD = \sqrt{\frac{\sum_{i=1}^{n} \left(\frac{\text{mod}_i}{\text{exp}_i} - \frac{\text{mod}_{avg}}{\text{exp}_{avg}} \right)^2}{n-1}} \tag{5}$$

As seen in Tables 6 and 7, all of the investigated models tend to estimate axial strength of FRP confined HPFRCC specimens in a good agreement. Particularly, Lam and Teng (2003) and Ilki et al. (2008) were extremely good in terms of axial strength predictions. However, when the ultimate strain prediction performances are considered, these two models, especially Ilki et al. (2008) heavily overestimated experimental values. Overestimation was observed mostly on rectangular specimens. The main reason of this overestimation can be attributed to the fact that, these two models are developed considering NSC specimens. On the other hand, as aforementioned in the presented study, strain efficiency factor was obtained as 0.30 for all cross sections in case of confinement of HPFRCC with CFRP sheets. However, these two models recommended higher strain efficiency factors resulting overestimation of test values. Similarly, Berthet et al. (2006), Wu et al. (2009) and Lim and Ozbakkaloglu (2013) exhibited satisfactory predictions in terms of ultimate strains, because they were developed considering HSC behavior. It is noteworthy that there is no model in the literature directly applicable to noncircular HSC or HPFRCC. Therefore, none of the 3 models (Berthet et al. (2006), Wu et al. (2009) and Lim and Ozbakkaloglu (2013)) developed considering HSC behavior was validated for noncircular specimens. As seen in Fig. 5a, these models have significantly good performance in predicting ultimate strain for circular specimens. In the light of analytical comparison of model performances, it may be considered that, when FRP volumetric ratio is increased using larger amount of CFRP layers, particularly in terms of strain enhancements, overestimations are going to be more important.

Table 5. Axial strength and ultimate strain prediction expressions of investigated models

Model	Axial strength expression	Ultimate axial strain expression	Definition of symbols
Lam and Teng (2003)	$\frac{f_{cc}^{'}}{f_{co}^{'}}=1+3.3k_{s1}\frac{f_{lu}^{(\psi)}}{f_{co}^{'}}$	$\frac{\varepsilon_{cu}}{\varepsilon_{co}}=1.75+12k_{s2}\frac{f_{lu}}{f_{co}^{'}}(\frac{\varepsilon_{h,rup}}{\varepsilon_{co}})^{0.45}$	$k_{s1}^{\partial}=(\frac{b}{h})^2(\frac{Ae}{Ac})^{(*)};k_{s2}=(\frac{b}{h})^{0.5}(\frac{Ae}{Ac});\mathrm{h}\geq\mathrm{b};k_{\varepsilon}=0.586$
Berthet et al. (2006)	$\frac{f_{cc}^{'}}{f_{co}^{'}}=1+\frac{k_1}{f_{co}^{'}}f_{lu}$	$\frac{\varepsilon_{cu}}{\varepsilon_{co}}=1+\frac{\sqrt{2}}{\varepsilon_{co}}(\frac{E_l^{\lambda}}{f_{co}^{'2}})^{2/3}(\varepsilon_f-\upsilon_c\varepsilon_{co})$	$k_1=\frac{9.5}{f_{co}^{'1/4}};\upsilon_c=0.2;k_{\varepsilon}=1$
Ilki et al. (2008)	$\frac{f_{cc}^{'}}{f_{co}^{'}}=[1+2.54(\frac{f_{l\max}^{'}}{f_{co}^{'}})]$	$\frac{\varepsilon_{cu}}{\varepsilon_{co}}=[1+(\frac{h}{b})19.27(\frac{f_{l\max}^{'}}{f_{co}^{'}})^{0.53}]$	$k_{\varepsilon}=0.85$
Wu et al. (2009)	$\frac{f_{cc}^{'}}{f_{co}^{'}}=1+3.2\frac{f_{lu}}{f_{co}^{'}}$	$\frac{\varepsilon_{cu}}{\varepsilon_{co}}=1+9.5\frac{f_{lu}}{f_{co}^{'}}$	$k_{\varepsilon}=1$
Lim and Ozbakkaloglu (2013)	$f_{cc}^{'}=c_1f_{co}^{'}+3.52(f_{lu}-f_{1o})$	$\varepsilon_{cu}=c_2\varepsilon_{co}+0.272(E_l/f_{co}^{'})\varepsilon_{h,rup}^{1.35}$ $\varepsilon_{co}=(-0.67f_{co}^{'2}+29.9f_{co}^{'}+1053)10^{-6}$	$c_1=1+0.0058E_l/f'_{co};\mathrm{f}_{1o}=E_l\varepsilon_{co}(0.43+0.009E_l/f'_{co})(E_l\geq K_{1o}^{(\dagger)})$ $c_1=(E_l/f_{co}^{'1.6})^{0.2};f_{1o}=24E_l\varepsilon_{co}(f'_{co}/E_l^{1.6})^{0.4}(E_l\geq K_{1o});c_2=2-(\frac{f'_{co}-20}{100})$

$(\psi)\ f_{lu}=\frac{2E_{frp}\varepsilon_{h,rup}t_f}{D}$ (*) $\frac{A_e}{A_c}=1-((b-2r)^2+(h-2r)^2/3A_g);\mathrm{A_g}=bh-(4-\pi)r^2$; $(\partial)k_{s1}=1;k_{s2}=1;k_{\varepsilon}=0.63$ *for circular* (for Lam and Teng 2003)

$(\lambda)\ E_l=\frac{f_{lu}}{\varepsilon_{h,rup}}$ (†) $K_{1o}=f_{co}^{1.65}$; $k_{\varepsilon}=0.9-2.3f'_{co}10^{-3}-0.75E_f10^{-6}$ (for Lim and Ozbakkaloglu 2013)

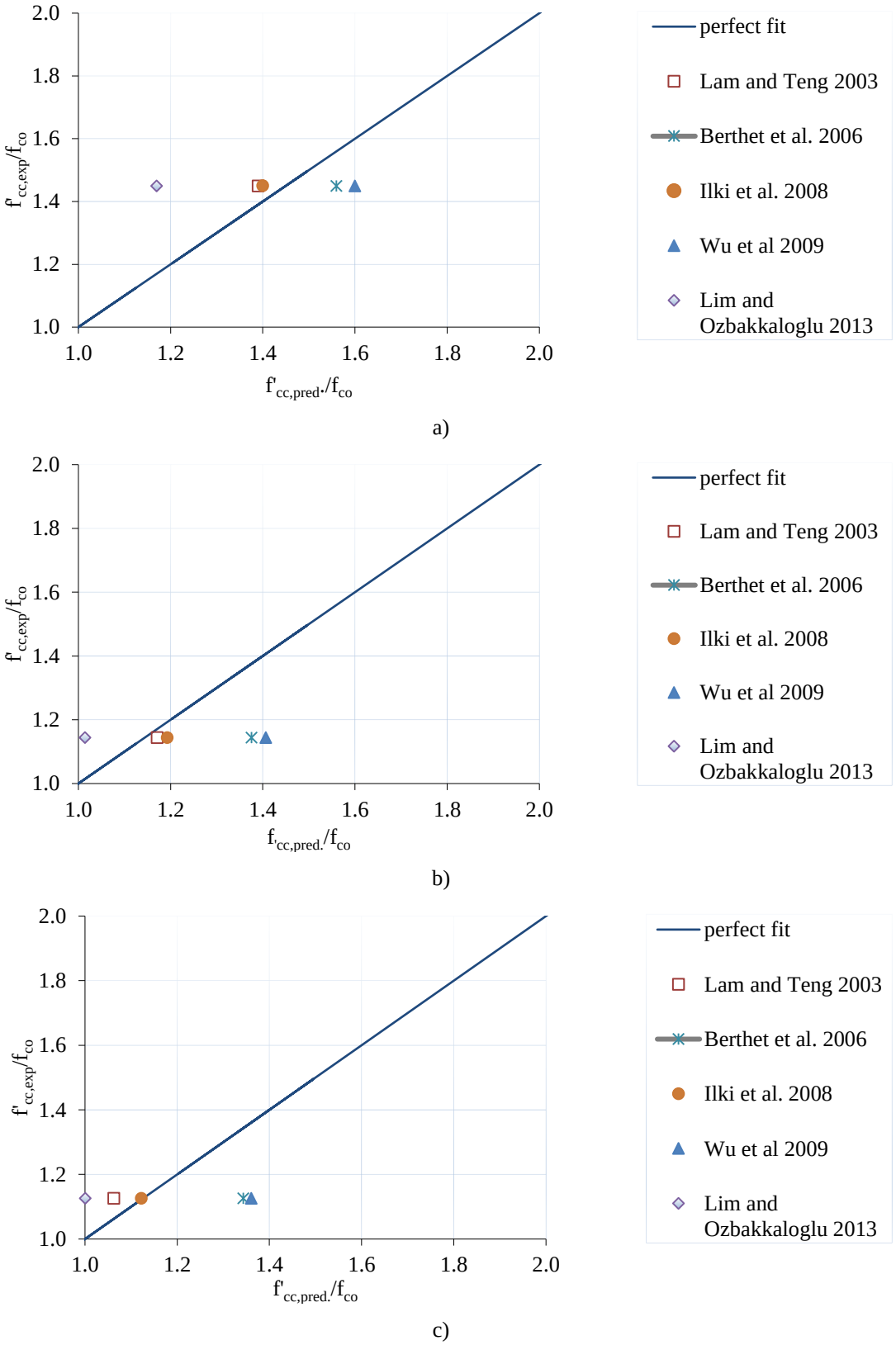

Fig. 4. Axial strength predictions of existing models for a) circular b) square and c) rectangular specimens

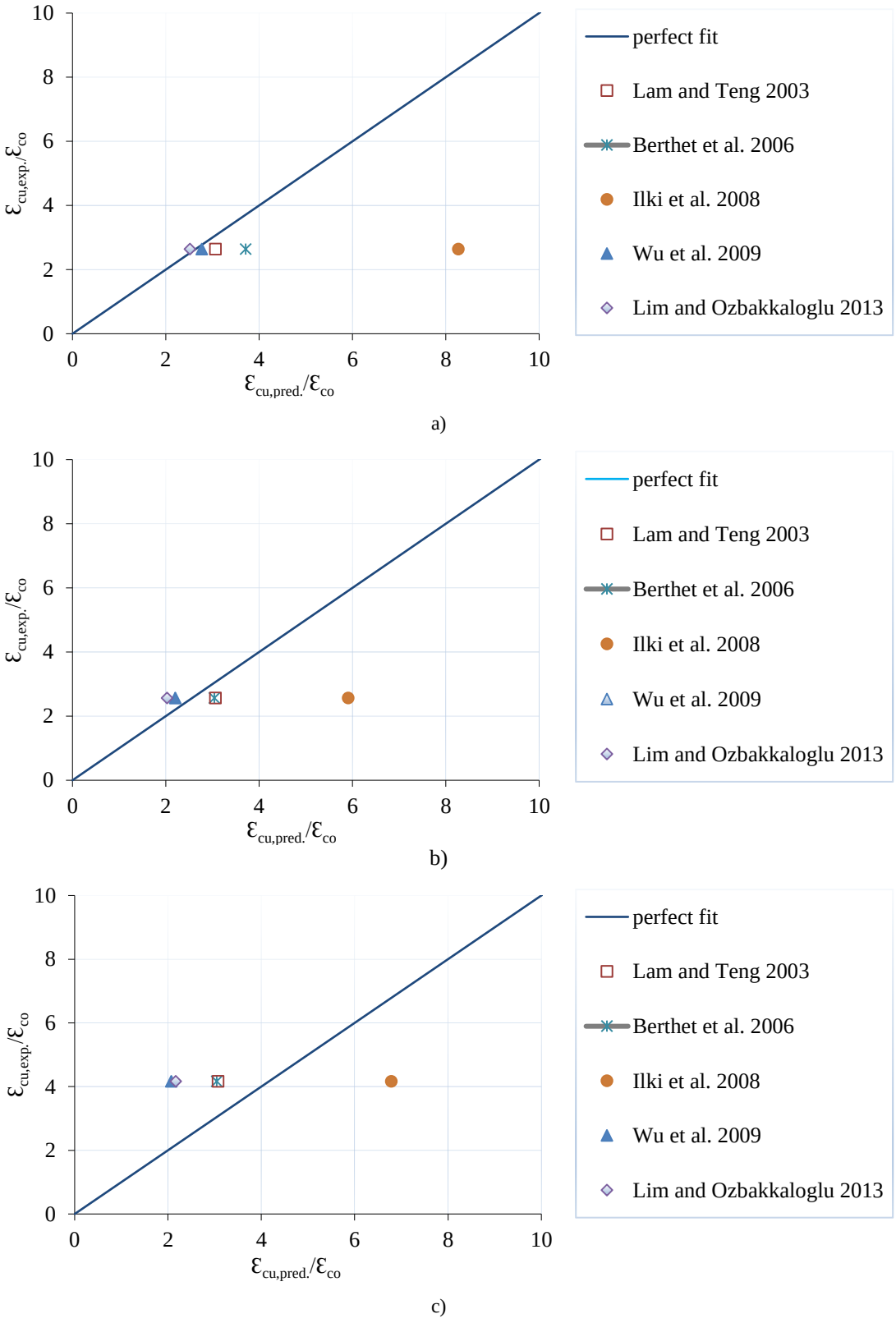

Fig. 5. Ultimate strain predictions of existing models for a) circular, b) square and c) rectangular specimens

Table 6. Statistics on investigated model performances

Model	f'_{cu}/f'_{co}		$\varepsilon_{cu}/\varepsilon_{co}$	
	AAE	*SD*	*AAE*	*SD*
Lam and Teng (2003)	0.02	0.03	0.21	0.37
Berthet et al. (2006)	0.08	0.09	0.14	0.23
Ilki et al. (2008)	0.01	0.02	0.68	0.93
Wu et al. (2009)	0.09	0.11	0.12	0.23
Lim and Ozbakkaloglu (2013)	0.07	0.08	0.12	0.22

Table 7. Categories of investigated model performances

Models	Category I		Category II		Category III	
	Strength	Strain	Strength	Strain	Strength	Strain
Lam and Teng (2003)	√			√		
Berthet et al. (2006)	√	√				
Ilki et al. (2008)	√					√
Wu et al. (2009)	√	√				
Lim and Ozbakkaloglu (2013)	√	√				

In order to make the axial behavior of CFRP confined HPFRCC more reliable, toughness and dilation behavior should also be investigated besides testing the specimens confined by more amounts of CFRP layers. In case of using more remarkable confinement levels resulting a second peak in stress-strain curve, post-peak strength loss might be eliminated as well.

4 CONCLUSIONS

On the basis of an experimental work of unconfined and CFRP confined circular, square and rectangular HPFRCC specimens, the following conclusions can be drawn:

1. When confined with CFRP sheets, the axial strength and ultimate strain capacity of the HPFRCC specimens are enhanced significantly. Strength enhancement can be pronounced more for confined circular specimens, while deformation capacity is observed more remarkable for rectangular ones.
2. A strain efficiency factor of 0.30 and average lateral strain value of 0.006 were obtained for HPFRCC confined by FRP sheets. These values are both observed to be less with respect to FRP confined NSC. The reason is attributed to the fact that in HPFRCC, increase in compressive strength caused a decrease in dilation capacity with respect to NSC. This behavior resulted lower lateral strains and strain efficiency factors in the case of FRP confined HPFRCC.
3. All of the investigated models made satisfactory predictions in terms of axial strength. The predictions of three models (Berthet et al. (2006), Wu et al. (2009) and Lim and Ozbakkaloglu (2013)) were in good agreement with experimentally obtained ultimate strains. However, this conclusion should be validated for other different cases. Therefore, further work is required considering higher/lower volumetric FRP ratios, toughness and dilation behavior of FRP confined HPFRCC.

REFERENCES

Almusallam, T.H. (2007). "Behavior of normal and high-strength concrete cylinders confined with Eglass/epoxy composite laminates." Composites Part B: Engineering, 38, 629 - 639.

Berthet, J. F., Ferrier, E. and Hamelin, P. (2006). "Compressive behavior of concrete externally confined by composite jackets: Part B: Modeling." Construction and Building Materials, 20(5), 338-347.

Brandt, A. M. (2008). "Fibre reinforced cement-based (FRC) composites after over 40 years of development in building and civil engineering." Composite Structures, 86(1), 3-9.

Dai, J. G., Bai, Y. L. and Teng, J. G. (2011). "Behavior and modeling of concrete confined with FRP composites of large deformability." Journal of Composites for Construction, 15(6), 963-973.

Ilki, A., Kumbasar, N. and Koc, V. (2002). "Strength and deformability of low strength concrete confined by carbon fiber composite sheets." 15th ASCE Engineering Mechanics Conference, New York, USA.

Ilki, A., Kumbasar, N. and Koc, V. (2004). "Low strength concrete members externally confined with FRP sheets." Structural Engineering and Mechanics, 18(2), 167-194.

Ilki, A., Peker, O., Karamuk, E., Demir, C. and Kumbasar, N. (2008). "FRP retrofit of low and medium strength circular and rectangular reinforced concrete columns." ASCE Journal of Materials in Civil Engineering, 20(2), 169-188.

Lam, L. and Teng, J. G. (2003). "Design-oriented stress-strain model for FRP confined concrete in rectangular columns." Journal of Reinforced Plastics and Composites, 22(13), 1149-1186.

Lam, L. and Teng, J.G. (2002). "Strength models for fiber-reinforced plastic confined concrete." Journal of Structural Engineering, 5, 612-623.

Lim, J. C. and Ozbakkaloglu, T. (2013). "Confinement model for FRP-confined high-strength concrete." Journal of Composites for Construction, 18(4), 04013058.

Mandal, S., Hoskin, A. and Fam, A. (2005). "Influence of concrete strength on confinement effectiveness of fiber-reinforced polymer circular jackets." ACI Structural Journal, 102(3), 383-392.

Ozbakkaloglu, T. (2012). "Axial compressive behavior of square and rectangular high-strength concrete-filled FRP tubes." Journal of Composites for Construction, 17(1), 151-161.

Ozbakkaloglu, T., Gholampour, A. and Lim, J. C. (2016). "Damage-plasticity model for FRP-confined normal-strength and high-strength concrete." Journal of Composites for Construction,

Teng, J. G., Chen, J. F., Smith, S. T. and Lam, L. (2002). "FRP strengthened RC structures." Wiley, New York.

Wang, D. Y., Wang, Z. Y., Smith, S. T. and Yu, T. (2016). "Size effect on axial stress-strain behavior of CFRP-confined square concrete columns." Construction and Building Materials, 118, 116-126.

Wu, H., Wang, Y., Yu, L. and Li, X. (2009). "Experimental and computational studies on high-strength concrete circular columns confined by aramid fiber-reinforced polymer sheets." Journal of Composites for Construction, 13(2), 125-134.

Wu, Y. F. and Zhou, Y. W. (2010). "Unified strength model based on Hoek-Brown failure criterion for circular and square concrete columns confined by FRP." Journal of Composites for Construction, 14(2), 175-184.

Xie, T. and Ozbakkaloglu, T. (2015). "Behavior of steel fiber-reinforced high-strength concrete-filled FRP tube columns under axial compression." Engineering Structures, 90, 158-171.

Zohrevand, P. and Mirmiran, A. (2012). "Behavior of ultra-high-performance concrete confined by fiber-reinforced polymers." ASCE Journal of Materials in Civil Engineering, 23(12), 1727-1734.